PROCEEDINGS

International Europhysics Conference on HEP

Measurement of CC interactions produced by ^{8}B solar neutrinos at SNO

Art McDonald[*†]

Department of Physics, Queen's University, Kingston, Ontario, Canada K7L 3N6
E-mail: mcdonald@sno.phy.queensu.ca

J. Boger, R.L. Hahn, J.K. Rowley, M. Yeh

Chemistry Department, Brookhaven National Laboratory, Upton, NY 11973-5000.

I. Blevis, F. Dalnoki-Veress, J. Farine, D.R. Grant, C.K. Hargrove, I. Levine, K. McFarlane, H. Mes, C. Mifflin, A.J. Noble, V.M. Novikov, M. O'Neill, M. Shatkay, D. Sinclair, N. Starinsky

Carleton University, Ottawa, Ontario K1S 5B6 Canada.

G. Milton, B. Sur

Atomic Energy of Canada Limited, Chalk River Laboratories, Chalk River, Ontario K0J 1J0.

J. Bigu, J.H.M. Cowan, E.D. Hallman, R.U. Haq, J. Hewett, J.G. Hykawy, G. Jonkmans, S. Luoma, A. Roberge, E. Saettler, M.H. Schwendener, H. Seifert, R. Tafirout, C.J. Virtue

Department of Physics and Astronomy, Laurentian University, Sudbury, Ontario P3E 2C6 Canada.

Y.D. Chan, X. Chen, M.C.P. Isaac, K.T. Lesko, A.D. Marino, E.B. Norman, C.E. Okada, A.W.P. Poon, A. Schuelke, A.R. Smith, R.G. Stokstad

Institute for Nuclear and Particle Astrophysics and Nuclear Science Division, Lawrence Berkeley National Laboratory, Berkeley, CA 94720.

T.J. Bowles, S.J. Brice, M.R. Dragowsky, M.M. Fowler, A. Goldschmidt, A. Hamer, A. Hime, K. Kirch, G.G. Miller, P. Thornewell, J.B. Wilhelmy, J.M. Wouters

Los Alamos National Laboratory, Los Alamos, NM 87545.

J.D. Anglin, M. Bercovitch, W.F. Davidson, R.S. Storey[‡]

National Research Council of Canada, Ottawa, Ontario K1A 0R6 Canada.

J.C. Barton, S. Biller, R.A. Black, R.J. Boardman, M.G. Bowler, J. Cameron, B.T. Cleveland, X. Dai, G. Doucas, J. Dunmore, H. Fergani, A.P. Ferraris, K. Frame, H. Heron, N.A. Jelley, A.B. Knox, M. Lay, W. Locke,J. Lyon, S. Majerus, N. McCauley, G. McGregor, M. Moorhead, M. Omori, N.W. Tanner, R.K. Taplin, M. Thorman, P.T. Trent, D.L. Wark, N. West, J. Wilson

Nuclear and Astrophysics Laboratory, University of Oxford, Keble Road, Oxford, OX1 3RH, UK

R. Kouzes, M.M. Lowry

Department of Physics, Princeton University, Princeton, NJ 08544

E. Bonvin, M.G. Boulay, M. Chen, E.T.H. Clifford, Y. Dai, F.A. Duncan, E.D. Earle, H.C. Evans, G.T. Ewan, R.J. Ford, A.L. Hallin, P.J. Harvey, R. Heaton, J.D. Hepburn, C. Jillings, H.W. Lee, J.R. Leslie, H.B. Mak, A.B. McDonald, W. McLatchie, B.A. Moffat,T.J. Radcliffe, B.C. Robertson, P. Skensved

Department of Physics, Queen's University, Kingston, Ontario K7L 3N6 Canada

S. Gil, J. Heise, R.L. Helmer, R.J. Komar, T. Kutter, C.W. Nally, H.S. Ng, Y.I. Tserkovnyak, C.E. Waltham

Department of Physics and Astronomy, University of British Columbia, Vancouver, BC V6T 1Z1 Canada

R.C. Allen, G. Bühler H.H. Chen[‡]

Department of Physics, University of California, Irvine, CA 92717

T.C. Andersen, K. Cameron, M.C. Chon, P. Jagam, J. Karn, J. Law,I.T. Lawson, R.W. Ollerhead, J.J. Simpson, N. Tagg, J.-X. Wang

Physics Department, University of Guelph, Guelph, Ontario N1G 2W1 Canada

E.W. Beier, D.F. Cowen, E.D. Frank, W. Frati, W.J. Heintzelman, P.T. Keener, J.R. Klein, C.C.M. Kyba, D.S. McDonald, M.S. Neubauer, F.M. Newcomer,S.M. Oser, V.L. Rusu,R. Van Berg, R.G. Van de Water, P. Wittich,

Department of Physics and Astronomy, University of Pennsylvania, Philadelphia, PA 19104-6396.

Q.R. Ahmad, M.C. Browne, T.V. Bullard, T.H. Burritt, G.A. Cox, P.J. Doe C.A. Duba, S.R. Elliott, J.V. Germani, A.A. Hamian, R. Hazama, K.M. Heeger, M. Howe, R. Meijer Drees, J.L. Orrell, R.G.H. Robertson, K.K. Schaffer, M.W.E. Smith, T.D. Steiger, J.F. Wilkerson

Center for Experimental Nuclear Physics and Astrophysics, and Department of Physics, University of Washington, Seattle, WA 98195

ABSTRACT: The Sudbury Neutrino Observatory (SNO) is a 1000 tonne heavy water Cherenkov detector placed 2 km underground in Ontario, Canada. Its main purpose is the detection of solar neutrinos, but it is also sensitive to atmospheric and supernova neutrinos. In this paper we report our first measurement of the solar electron-type neutrino flux using the charged current interaction on deuterium, above an electron kinetic energy threshold of 6.75 MeV. This measurement, when compared with an electron scattering measurement from Super Kamiokande, provides the first evidence for non-electron neutrino types from the Sun implying flavor change of solar electron neutrinos. We also present an initial angular distribution of through-going muons, which shows that we can detect neutrino-induced muons from well above the horizontal. This will give us good sensitivity to neutrino oscillations in the atmospheric sector.

1. Solar Neutrinos

1.1 Introduction

Solar neutrino experiments over the past 30 years [1, 2, 3, 4, 5, 6] have measured fewer neutrinos than are predicted by models of the Sun [7, 8]. One explanation for the deficit is the transformation of the Sun's electron-type neutrinos into other active flavours. The Sudbury Neutrino Observatory measures the ^{8}B solar neutrinos through the reactions:

$$\begin{aligned} \nu_e + d &\rightarrow p + p + e^- && \text{(CC)} \\ \nu_x + d &\rightarrow p + n + \nu_x && \text{(NC)} \\ \nu_x + e^- &\rightarrow \nu_x + e^- && \text{(ES)} \end{aligned}$$

The charged current reaction (CC) is sensitive exclusively to electron-type neutrinos, while the neutral current (NC) is sensitive to all active neutrino flavours ($x = e, \mu, \tau$). The elastic scattering (ES) reaction is sensitive to all flavours as well, but with reduced sensitivity to ν_μ and ν_τ. By itself, the ES reaction cannot provide a measure of the total ^{8}B flux or its flavour content. Comparison of the ^{8}B flux deduced from the ES reaction assuming no neutrino oscillations ($\phi^{\mathrm{ES}}(\nu_x)$), to that measured by the CC reaction ($\phi^{\mathrm{CC}}(\nu_e)$) can provide clear evidence of flavour transformation without reference to solar model flux calculations. If neutrinos from the Sun change into other active flavours, then $\phi^{\mathrm{CC}}(\nu_e) < \phi^{\mathrm{ES}}(\nu_x)$.

The SNO experimental plan calls for three phases of about one year each wherein different techniques will be employed for the detection of neutrons from the NC reaction. During the first phase, with pure heavy water, neutrons are observed through the Cerenkov light produced when neutrons are captured in deuterium, producing 6.25 MeV gammas. In this phase, the capture probability for such neutrons is about 25% and the Cerenkov light is relatively close to the threshold of about 5 MeV electron energy, imposed by radioactivity

*Speaker.

†for the SNO Collaboration

‡deceased

in the detector. (Figure 1). For the second phase, about 2.5 tonnes of NaCl will be added to the heavy water and neutron detection will be enhanced through capture on Cl, with about 8.6 MeV gamma energy release and about 83% capture efficiency. (See Figure 1). For the third phase, the salt is removed and an array of ^{3}He- filled proportional counters will be installed to provide direct detection of neutrons with a capture efficiency of about 45%.

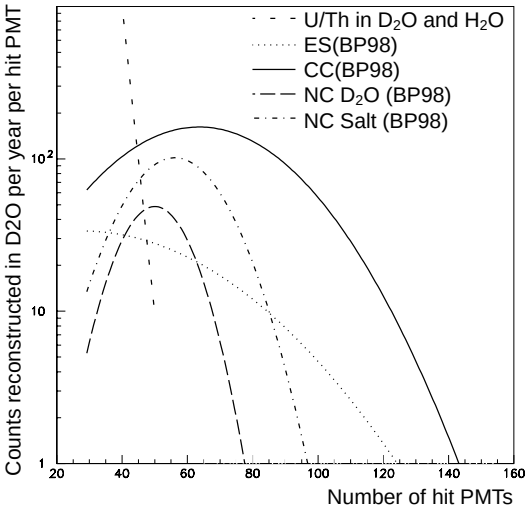

Figure 1: Simulations of spectra obtained from the three detection reactions (CC,ES,NC)for neutrino fluxes as calculated [9] by BP98. Spectra from the NC reaction are shown for pure heavy water and with added salt. The expected counting rate from U and Th radioactivity in the water is also shown. An MeV of electron energy corresponds to about 9 photomultipliers (PMT's) hit.

1.2 First Experimental Results

We present the first results from SNO on the ES and CC reactions. SNO's measurement of $\phi^{\rm ES}(\nu_x)$ is consistent with previous measurements described in Ref [5]. The measurement of $\phi^{\rm CC}(\nu_e)$, however, is significantly smaller and is therefore inconsistent with the null hypothesis that all observed solar neutrinos are ν_e. A measurement using the NC reaction, which has equal sensitivity to all neutrino flavours, will be reported in a future publication.

SNO [10] is an imaging water Cherenkov detector located at a depth of 6010 m of water equivalent (m.w.e) in the INCO, Ltd Creighton mine near Sudbury, Ontario. It features 1000 metric tons of ultra-pure D_2O contained in a 12 m diameter spherical acrylic vessel. This sphere is surrounded by a shield of ultra-pure H_2O contained in a 34 m high barrel-shaped cavity of maximum diameter 22 m. A stainless steel structure 17.8 m in diameter supports 9456 20-cm photomultiplier tubes (PMTs) with light concentrators. Approximately 55% of the light produced within 7 m of the centre of the detector will strike a PMT.

1.3 Data Analysis

The data reported here were recorded between Nov. 2, 1999 and Jan. 15, 2001 and correspond to a live time of 240.95 days. Events are defined by a multiplicity trigger of 18 or more PMTs exceeding a threshold of ~ 0.25 photo-electrons within a time window of 93 ns. The trigger reaches 100% efficiency at 23 PMTs. The total instantaneous trigger rate is 15-18 Hz, of which 6-8 Hz is the data trigger. For every event trigger, the time and charge responses of each participating PMT are recorded.

The data were partitioned into two sets, with approximately 70% used to establish the data analysis procedures and 30% reserved for a blind test of statistical bias in the

analysis. The analysis procedures were frozen before the blind data set was analyzed, and no statistically significant differences in the data sets were found. We present here the analysis of the combined data sets.

Calibration of the PMT time and charge pedestals, slopes, offsets, charge vs. time dependencies, and second order rate dependencies are performed using electronic pulsers and pulsed light sources. Optical calibration is obtained using a diffuse source of pulsed laser light at 337, 365, 386, 420, 500 and 620 nm. The absolute energy scale and uncertainties are established with a triggered ^{16}N source (predominantly 6.13-MeV γ's) deployed over two planar grids within the D_2O and a linear grid in the H_2O. The resulting Monte Carlo predictions of detector response are tested using a ^{252}Cf neutron source, which provides an extended distribution of 6.25-MeV γ rays from neutron capture, and a ^{3}H$(p,\gamma)^4$He [11] source providing 19.8-MeV γ rays. The volume-weighted mean response is approximately nine PMT hits per MeV of electron energy.

The first step in the data reduction process is the elimination of instrumental backgrounds. Electrical pickup may produce false PMT hits, while electrical discharges in the PMTs or insulating detector materials produce light. These backgrounds have characteristics very different from Cherenkov light, and are eliminated using cuts based only on the PMT positions, the PMT time and charge data, event-to-event time correlations, and veto PMTs. This step in the data reduction is verified by comparing results from two independent background rejection analyses. For events passing the first stage, the calibrated times and positions of the hit PMTs are used to reconstruct the vertex position and the direction of the particle. The reconstruction accuracy and resolution are measured using Compton electrons from the ^{16}N source, and the energy and source variation of reconstruction are checked with a ^{8}Li β source. Angular resolution is measured using Compton electrons produced more than 150 cm from the ^{16}N source. At these energies, the vertex resolution is 16 cm and the angular resolution is 26.7 degrees.

An effective kinetic energy, $T_{\rm eff}$, is assigned to each event passing the reconstruction stage. $T_{\rm eff}$ is calculated using prompt (unscattered) Cherenkov photons and the position and direction of the event. The derived energy response of the detector can be characterized by a Gaussian:

$$R(E_{\rm eff}, E_e) = \frac{1}{\sqrt{2\pi}\sigma_E(E_e)} \exp[-\frac{1}{2}(\frac{E_{\rm eff} - E_e}{\sigma_E(E_e)})^2]$$

where E_e is the total electron energy, $E_{\rm eff} = T_{\rm eff} + m_e$, and $\sigma_E(E_e) = (-0.4620 + 0.5470\sqrt{E_e} + 0.008722E_e)$ MeV is the energy resolution. The uncertainty on the energy scale is found to be $\pm 1.4\%$, which results in a flux uncertainty nearly 4 times larger. For validation, a second energy estimator counts all PMTs hit in each event, N_{hit}, without position and direction corrections.

Further instrumental background rejection is obtained using reconstruction figures of merit, PMT time residuals, and the average angle between hit PMTs ($\langle\theta_{ij}\rangle$), measured from the reconstructed vertex. These cuts test the hypothesis that each event has the characteristics of single electron Cherenkov light. The effects of these and the rest of the instrumental background removal cuts on neutrino signals are quantified using the ^{8}Li and ^{16}N sources deployed throughout the detector. The volume-weighted neutrino signal loss

is measured to be $1.4^{+0.7}_{-0.6}\%$ and the residual instrumental contamination for the data set within the D_2O is $< 0.2\%$. Lastly, cosmic ray induced neutrons and spallation products are removed using a 20 s coincidence window with the parent muon.

In the remaining events above a threshold of $T_{\rm eff} \geq 6.75$ MeV, there are contributions from CC events in the D_2O, ES events in the D_2O and H_2O, a residual tail of neutron capture events, and high energy γ rays from radioactivity in the outer detector. The data show a clear signal within the D_2O volume. A fiducial volume cut is applied at $R = 5.50$ m to reduce backgrounds from regions exterior to the D_2O, and to minimize systematic uncertainties associated with optics and reconstruction near the acrylic vessel.

Possible backgrounds from radioactivity in the D_2O and H_2O are measured by regular low level radio-assays of U and Th decay chain products in these regions. The Cherenkov light character of D_2O and H_2O radioactivity backgrounds is used *in situ* to monitor backgrounds between radio-assays. Low energy radioactivity backgrounds are removed by the high threshold imposed, as are most neutron capture events. Monte Carlo calculations predict that the H_2O shield effectively reduces contributions of low energy (< 4 MeV) γ rays from the PMT array, and these predictions are verified by deploying an encapsulated Th source in the vicinity of the PMT support sphere. High energy γ rays from the cavity are also attenuated by the H_2O shield. A limit on their leakage into the fiducial volume is estimated by deploying the ^{16}N source near the edge of the detector's active volume. The total contribution from all radioactivity in the detector is found to be $<0.2\%$ for low energy backgrounds and $<0.8\%$ for high energy backgrounds.

1.4 Results

The final data set contains 1169 events after the fiducial volume and kinetic energy threshold cuts. Figure 2 (a) displays the distribution of $\cos\theta_\odot$, the angle between the reconstructed direction of the event and the instantaneous direction from the Sun to the Earth. The forward peak in this distribution arises from the kinematics of the ES reaction, while CC electrons are expected to have a distribution which is $(1 - 0.340\cos\theta_\odot)$ [12], before accounting for detector response.

The data are resolved into contributions from CC, ES, and neutron events above threshold using probability density functions (pdfs) in $T_{\rm eff}$, $\cos\theta_\odot$, and $(R/R_{\rm AV})^3$, generated from Monte Carlo simulations assuming no flavour transformation and the shape of the standard ^{8}B spectrum [13] (*hep* neutrinos are not included in the fit). The extended maximum likelihood method used in the signal extraction yields 975.4 ± 39.7 CC events, 106.1 ± 15.2 ES events, and 87.5 ± 24.7 neutron events for the fiducial volume and the threshold chosen, where the uncertainties given are statistical only. The dominant sources of systematic uncertainty in this signal extraction are the energy scale uncertainty and reconstruction accuracy, as shown in Table 1. The CC and ES signal decomposition gives consistent results when used with the N_{hit} energy estimator, as well as with different choices of the analysis threshold and the fiducial volume up to 6.20 m with backgrounds characterized by pdfs.

The CC spectrum can be extracted from the data by removing the constraint on the shape of the CC pdf and repeating the signal extraction.

Error source	CC error (percent)	ES error (per cent)
Energy scale	-5.2, +6.1	-3.5 ,+5.4
Energy resolution	±0.5	±0.3
Energy scale non-linearity	±0.5	±0.4
Vertex accuracy	±3.1	±3.3
Vertex resolution	±0.7	±0.4
Angular resolution	±0.5	±2.2
High energy γ's	-0.8, +0.0	-1.9, +0.0
Low energy background	-0.2, +0.0	-0.2, +0.0
Instrumental background	-0.2, +0.0	-0.6, +0.0
Trigger efficiency	0.0	0.0
Live time	±0.1	±0.1
Cut acceptance	-0.6, +0.7	-0.6, +0.7
Earth orbit eccentricity	±0.1	±0.1
^{17}O, ^{18}O	0.0	0.0
Experimental uncertainty	-6.2, +7.0	-5.7, +6.8
Cross section	3.0	0.5
Solar Model	-16, +20	-16, +20

Table 1: Systematic error on fluxes.

Figure 2 (b) shows the kinetic energy spectrum with statistical error bars, with the ^{8}B spectrum of Ortiz *et al.* [13] scaled to the data. The ratio of the data to the prediction [7] is shown in Figure 2 (c). The bands represent the 1σ uncertainties derived from the most significant energy-dependent systematic errors. There is no evidence for a deviation of the spectral shape from the predicted shape under the non-oscillation hypothesis.

Normalized to the integrated rates above the kinetic energy threshold of $T_{\rm eff} = 6.75$ MeV, the measured ^{8}B neutrino fluxes assuming the standard spectrum shape [13] are:

$$\phi^{\rm CC}_{\rm SNO}(\nu_e) = 1.75 \pm 0.07\ ({\rm stat.})^{+0.12}_{-0.11}\ ({\rm sys.}) \pm 0.05\ ({\rm theor.}) \times 10^6\ {\rm cm}^{-2}{\rm s}^{-1}$$
$$\phi^{\rm ES}_{\rm SNO}(\nu_x) = 2.39 \pm 0.34({\rm stat.})^{+0.16}_{-0.14}\ ({\rm sys.}) \times 10^6\ {\rm cm}^{-2}{\rm s}^{-1}$$

where the theoretical uncertainty is the CC cross section uncertainty [14]. Radiative corrections have not been applied to the CC cross section, but they are expected to decrease the measured $\phi^{\rm CC}(\nu_e)$ flux [15]by up to a few percent. The difference between the ^{8}B flux deduced from the ES rate and that deduced from the CC rate in SNO is $0.64 \pm 0.40 \times 10^6$ cm^{-2}s^{-1}, or 1.6σ. SNO's ES rate measurement is consistent with the precision measurement by the Super-Kamiokande Collaboration of the ^{8}B flux using the same ES reaction [5]:

$$\phi^{\rm ES}_{\rm SK}(\nu_x) = 2.32 \pm 0.03\ ({\rm stat.})^{+0.08}_{-0.07}\ ({\rm sys.}) \times 10^6\ {\rm cm}^{-2}{\rm s}^{-1}.$$

The difference between the flux $\phi^{\rm ES}(\nu_x)$ measured by Super-Kamiokande via the ES reaction and the $\phi^{\rm CC}(\nu_e)$ flux measured by SNO via the CC reaction is $0.57 \pm 0.17 \times 10^6$

$cm^{-2}s^{-1}$, or 3.3σ [16], assuming that the systematic errors are normally distributed. The probability that a downward fluctuation of the Super-Kamiokande result would produce a SNO result $\geq 3.3\sigma$ is 0.04%. For reference, the ratio of the SNO CC ^{8}B flux to that of the BPB01 solar model [7] is 0.347±0.029, where all uncertainties are added in quadrature.

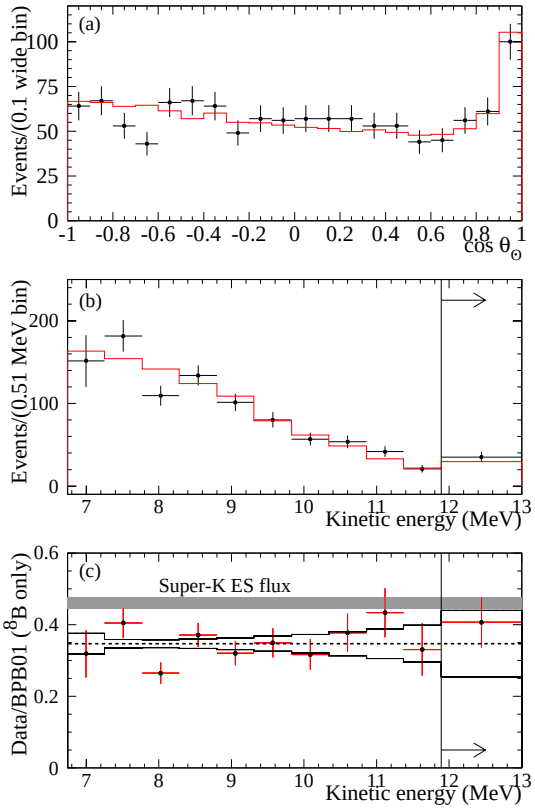

Figure 2: Distributions of (a) $\cos\theta_\odot$, and (b) extracted kinetic energy spectrum for CC events with R ≤5.50 m and $T_{\rm eff}$≥6.75 MeV. The Monte Carlo simulations for an undistorted ^{8}B spectrum are shown as histograms. The ratio of the data to the expected kinetic energy distribution with correlated systematic errors is shown in (c). The uncertainties in the ^{8}B spectrum have not been included.

1.5 Implications

If oscillation solely to a sterile neutrino is occurring, the SNO CC-derived ^{8}B flux above a threshold of 6.75 MeV will be consistent with the integrated Super-Kamiokande ES-derived ^{8}B flux above a threshold of 8.5 MeV[17]. Adjusting the ES threshold [5] this derived flux difference is $0.53 \pm 0.17 \times 10^6$ $cm^{-2}s^{-1}$, or 3.1σ. The probability of a downward fluctuation $\geq 3.1\sigma$ is 0.13%. These data are therefore evidence of a non-electron active flavour component in the solar neutrino flux. These data are also inconsistent with the "Just-So^2" parameters for neutrino oscillation [19].

Figure 3 displays the inferred flux of non-electron flavour active neutrinos ($\phi(\nu_{\mu\tau})$) against the flux of electron neutrinos. The two data bands represent the one standard deviation measurements of the SNO CC rate and the Super-Kamiokande ES rate. The error ellipses represent the 68%, 95%, and 99% joint probability contours for $\phi(\nu_e)$ and $\phi(\nu_{\mu\tau})$. The best fit to $\phi(\nu_{\mu\tau})$ is:

$$\phi(\nu_{\mu\tau}) = 3.69 \pm 1.13 \times 10^6 \text{ cm}^{-2}\text{s}^{-1}.$$

The total flux of active ^{8}B neutrinos is determined to be:

$$\phi(\nu_x) = 5.44 \pm 0.99 \times 10^6 \text{ cm}^{-2}\text{s}^{-1}.$$

This result is displayed as a diagonal band in Fig. 3, and is in excellent agreement with predictions of standard solar models [7, 8].

In summary, the results presented here are the first direct indication of a non-electron flavour component in the solar neutrino flux, and enable the first determination of the total flux of ^{8}B neutrinos generated by the Sun.

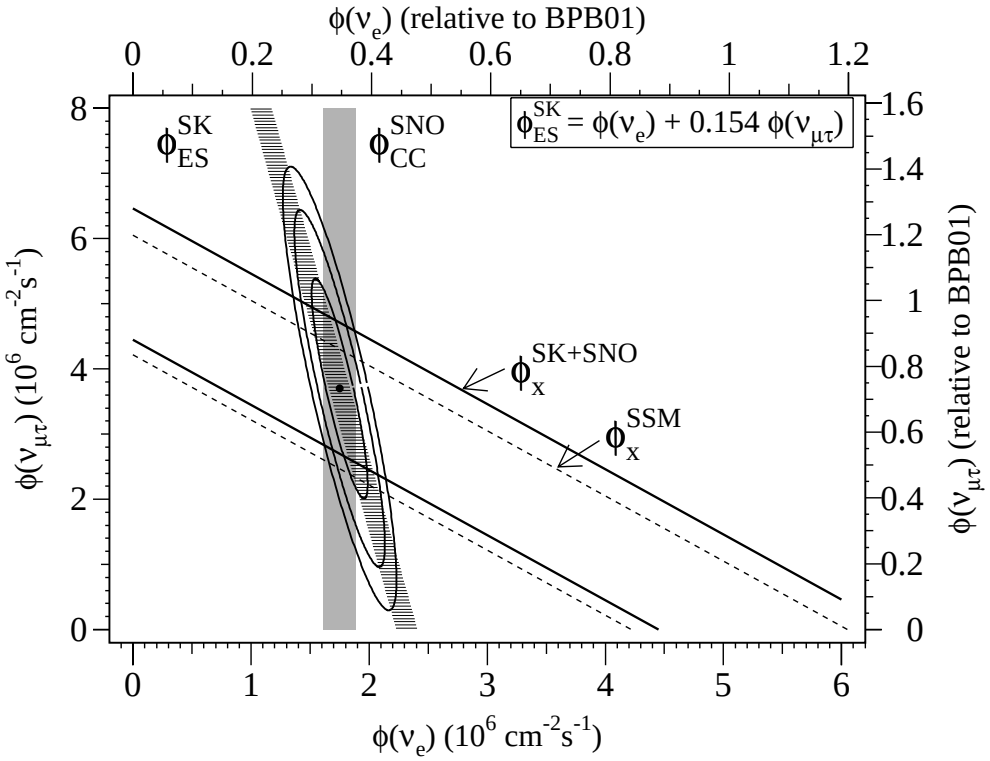

Figure 3: Flux of ^{8}B solar neutrinos which are μ or τ flavour vs. the flux of electron neutrinos as deduced from the SNO and Super-Kamiokande data. The diagonal bands show the total ^{8}B flux $\phi(\nu_x)$ as predicted by BPB01 (dashed lines) and that derived from the SNO and Super-Kamiokande measurements (solid lines). The intercepts of these bands with the axes represent the $\pm 1\sigma$ errors.

1.6 Future Work

Since June, 2001, the detector has been running with NaCl installed for the second phase of the project in which the sensitivity to the NC reaction is enhanced. The radioactivity levels throughout the first phase with pure heavy water were very low and these have been maintained for the second phase. Figure 4 shows the radioactivity levels in the heavy water as measured by direct extraction of radon from the water (top) or by extraction of radium from the Th (middle) or Uranium (bottom) chains using manganese dioxide or hydrous titanium oxide absorbers. The horizontal lines correspond to the levels for producing neutrons by the photodisintegration of deuterium at 5 percent of the number that would be produced by the NC reaction for a standard solar model flux. These levels have been met or exceeded.

Future analyses for solar neutrinos will include measurements of the NC reaction for pure heavy water and with salt inserted, measurements of all reactions versus zenith angle and various temporal periods.

2. Through-Going Muons

Muon events in SNO come from two sources. Some very high energy atmospheric muons

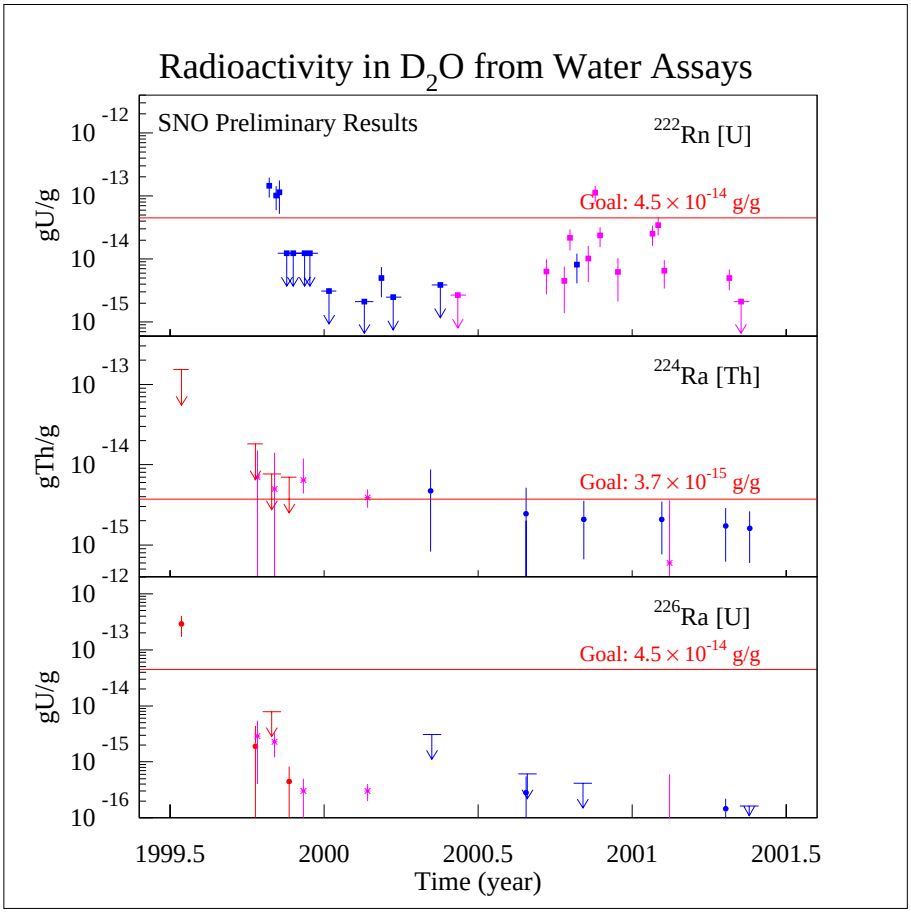

Figure 4: Measurements of radioactivity levels in the heavy water versus time. The horizontal lines are target levels as described in the text.

(>4 TeV) have sufficient energy to reach SNO if travelling almost vertically downward; the rate detected is about 3 per hour. Atmospheric muon neutrinos can interact with the rock around SNO. They produce penetrating muons which travel up to about 10 km.w.e. and can be detected by SNO. We expect and find the rate of detection of distinguishable neutrino-induced muons to be about 120/y. This rate is tiny compared with the downward muon rate, but SNO's angular resolution is sufficient to obtain a clean separation of the two sources at $\cos\theta \approx 0.4$. The mean minimum through-going muon energy is 2.9 GeV.

2.1 Neutrino-Induced Muons

Existing data on atmospheric neutrinos, of which neutrino-induced muons are a part, principally from Super-Kamiokande (SK) [25], point to a $\nu_\mu \rightarrow \nu_\tau$ oscillation with a mass difference squared of $\Delta m^2 \approx 0.003$ eV^2 and a mixing angle $\theta \approx 45$ deg. One signal for this oscillation is the angular distribution of neutrino-induced muons. The geometry of the earth implies that neutrinos with these parameters coming from above the horizon do not oscillate, but those coming from below the horizon do oscillate. This leads to a distortion of the zenith angular distribution, with the signal from below the horizon reduced by almost

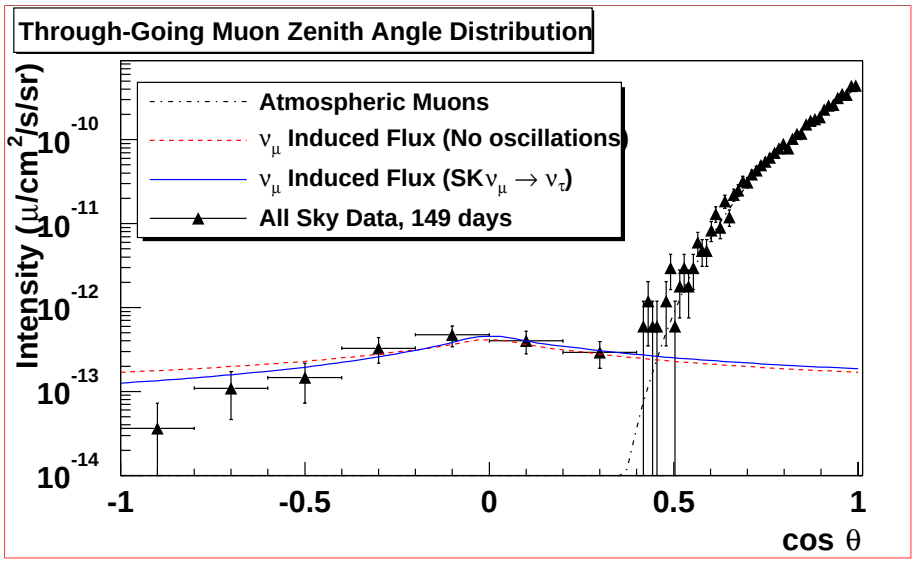

Figure 5: Complete zenith angle distribution of through-going muons. The theoretical curves are (i) downward muons ($\cos\theta > 0.4$) with the nominal surface distribution and propagation in rock calculated with MUSIC, (ii) neutrino-induced muons ($\cos\theta < 0.4$) with the Bartol neutrino flux, propagation in rock calculated with MUSIC, with (continuous line) and without (dashed line) oscillations. The overall neutrino flux is fitted to the data; the values of χ^2/d.f. are 6.29/6 for the no oscillation case and 3.90/6 for the preferred SK $\nu_\mu \rightarrow \nu_\tau$ oscillation parameters.

a factor two. Thus SNO's unique contribution to this area of neutrino oscillation physics is to detect both oscillated and unoscillated neutrino-induced through-going muons. Those seen coming from above the horizon provide a good test of the flux models, unhampered by oscillation effects. In effect we can make a self-normalizing measurement of the high energy atmospheric neutrino flux with a baseline of between 20 and 13,000 km. Without oscillations, the angular distribution is expected to be almost symmetrical above and below the horizontal. The only other effect which can disturb this symmetry is that of the geomagnetic field. However at SNO's high magnetic latitude [27] it can be shown that the primaries which give rise to through-going muons with $E > 2.9$ GeV experience very little distortion.

2.2 Through-Going Muon Analysis

We present here the analysis of 149 live days during the time from November 1999 to June 2000. To reconstruct muon position and direction from PMT times and charges required a model of Cherenkov light generation and an event fitter [26]. The r.m.s. angular error of the fitter was 2.1°, and the r.m.s. position error was 0.1 m. Events near the edge of the detector exhibited poor reconstruction (due to short contained track lengths) and so a cut on the impact parameter (radius of closest approach) was made, accepting all events that reconstructed within ∼7.5 m of the centre of the detector. The fiducial area, 175.5 m^2 was defined with an error of 2.65%. The final muon sample after these cuts consisted of 7579 events.

2.3 Horizontal and Upward Muons

Two theoretical calculations of neutrino-induced muons are shown in fig.5. In both we use the Bartol neutrino flux [22], but allow the overall normalization to float. There are two lines, one with and one without neutrino oscillations. In the oscillation case, we take $\sin^2 2\theta = 1$ and $\Delta m^2 = 0.003$ eV^2. The overall neutrino flux is fitted to the data; the values of χ^2/d.f. are 6.29/6 for the no oscillation case and 3.90/6 for the preferred SK $\nu_\mu \rightarrow \nu_\tau$ oscillation parameters. This result marginally favours the SK oscillation parameters. The previously unobserved signal above the horizon is as anticipated [26].

3. Acknowledgements

This research was supported by the Natural Sciences and Engineering Research Council of Canada, Industry Canada, National Research Council of Canada, Northern Ontario Heritage Fund Corporation and the Province of Ontario, the United States Department of Energy, and in the United Kingdom by the Science and Engineering Research Council and the Particle Physics and Astronomy Research Council. Further support was provided by Atomic Energy of Canada Limited (AECL), Agra-Monenco, Canatom, Canadian Microelectronics Corporation, AT&T Microelectronics, Northern Telecom and British Nuclear Fuels, Ltd. The heavy water was loaned by AECL with the cooperation of Ontario Power Generation.

We particularly thank INCO for the provision of SNO's underground site and for all the support provided to make the experiment possible.

References

[1] B.T. Cleveland *et al.*, Astrophys. J. **496**, 505 (1998).

[2] K.S. Hirata *et al.*, Phys. Rev. Lett. **65**, 1297 (1990); K.S. Hirata *et al.*, Phys. Rev. D **44**, 2241 (1991), **45** 2170E (1992); Y. Fukuda *et al.*, Phys. Rev. Lett. **77**, 1683 (1996).

[3] J.N. Abdurashitov *et al.*, Phys. Rev. C **60**, 055801, (1999).

[4] W. Hampel *et al.*, Phys. Lett. B **447**, 127 (1999).

[5] S. Fukuda *et al.*, Phys. Rev. Lett. **86**, 5651 (2001).

[6] M. Altmann *et al.*, Phys. Lett. B **490**, 16 (2000).

[7] J.N. Bahcall, M. H. Pinsonneault, and S. Basu, astro-ph/0010346 v2. The reference ^{8}B neutrino flux is 5.05×10^6 cm^{-2}s^{-1}.

[8] A.S. Brun, S. Turck-Chièze, and J.P. Zahn, Astrophys. J. **525**, 1032 (1999); S. Turck-Chièze *et al.*, Ap. J. Lett., v. **555** July 1, 2001.

[9] J.N. Bahcall, S. Basu and M. H. Pinsonneault, Phys. Lett. B433 (1998) 1.

[10] The SNO Collaboration, Nucl. Instr. and Meth. **A449**, 172 (2000).

[11] A.W.P. Poon *et al.*, Nucl. Instr. and Meth. **A452**, 115, (2000).

[12] J.F. Beacom and P. Vogel, hep-ph/9903554, Phys. Rev. Lett. **83**, 5222 (1999).

[13] C.E. Ortiz *et al.*, Phys. Rev. Lett. **85**, 2909 (2000).

[14] S. Nakamura, T. Sato, V. Gudkov, and K. Kubodera, Phys. Rev. C **63**, 034617 (2001); M. Butler, J.-W. Chen, and X. Kong, Phys. Rev. C **63**, 035501 (2001); G. 't Hooft, Phys. Lett. **37B** 195 (1971). The Butler *et al.* cross section with $L_{I,A} = 5.6$ fm^3 is used.

[15] I. S. Towner, J. Beacom, and S. Parke, private communication; I. S. Towner, Phys. Rev. C **58** 1288 (1998), J. Beacom and S. Parke, hep-ph/0106128; J.N. Bahcall, M. Kamionkowski, and A. Sirlin, Phys. Rev. D **51** 6146 (1995).

[16] Given the limit set for the *hep* flux by Ref. [5], the effects of the *hep* contribution may increase this difference by a few percent.

[17] G. L. Fogli, E. Lisi, A. Palazzo, and F.L. Villante Phys. Rev. D **63**, 113016 (2001); F.L. Villante, G. Fiorentini and E. Lisi Phys. Rev. D **59** 013006 (1999).

[18] M. Apollonio *et al.*, Phys. Lett. B **466**, 415 (1999).

[19] J.N. Bahcall, P.I. Krastev, and A.Yu. Smirnov, JHEP **05**, 015 (2001).

[20] T. Toshito *et al.* hep-ex/0105023 European Physical Journal **C15**, 1 (2000)

[21] J. Bonn *et al.* Nucl. Phys. Proc. B Suppl. **91**, 273 (2001).

[22] V. Agrawal, T. K. Gaisser, P. Lipari and T. Stanev, Phys. Rev. D **53**, (1996) 1314.

[23] J.F. Beacom, R.N. Boyd, and A. Mezzacappa; Phys. Rev. Lett. **85** (2000) 3568-3571.

[24] A. Burrows; Nature **403** (2000) 727-733.

[25] S. Fukuda *et al.*, Phys. Rev. Lett. **86**, 5651 (2001).

[26] N. Tagg, Ph.D thesis, University of Guelph (2001), unpublished. Available on http://www.sno.phy.queensu.ca/sno/publications.html.

[27] Y. I. Tserkovnyak et al, Proceedings of ICRC2001, Hamburg, Germany.

[28] P. Vogel and J.F. Beacom; Phys. Rev. **D60** (1999) 053003.